



Research
Material Engineering—Article

Bifunctional Asymmetric Fabric with Tailored Thermal Conduction and Radiation for Personal Cooling and Warming

Yucan Peng^a, Hiang Kwee Lee^a, David S. Wu^a, Yi Cui^{a,b,*}

^a Department of Materials Science and Engineering, Stanford University, Stanford, Menlo Park, CA 94305, USA

^b Stanford Institute for Materials and Energy Sciences, SLAC National Accelerator Laboratory, Menlo Park, CA 94025, USA



ARTICLE INFO

Article history:

Received 18 January 2021

Revised 30 March 2021

Accepted 30 April 2021

Available online 28 May 2021

Keywords:

Textiles

Personal thermal management

Bifunctional asymmetric fabric

Heat conduction

Radiative heat transfer

ABSTRACT

Personal thermal management is emerging as a promising strategy to provide thermal comfort for the human body while conserving energy. By improving control over the heat dissipating from the human body, personal thermal management can provide effective personal cooling and warming. Here, we propose a facile surface modification approach to tailor the thermal conduction and radiation properties based on commercially available fabrics, to realize better management of the whole heat transport pathway from the human body to the ambient. A bifunctional asymmetric fabric (BAF) offering both a cooling and a warming effect is demonstrated. Due to the advantages of roughness asymmetry and surface modification, the BAF demonstrates an effective cooling effect through enhanced heat conduction and radiation in the cooling mode; in the warming mode, heat dissipation along both routes is reduced for personal warming. As a result, a 4.6 °C skin temperature difference is measured between the cooling and warming BAF modes, indicating that the thermal comfort zone of the human body can be enlarged with one piece of BAF clothing. We expect this work to present new insights for the design of personal thermal management textiles as well as a novel solution for the facile modification of available fabrics for both personal cooling and warming.

© 2021 THE AUTHORS. Published by Elsevier LTD on behalf of Chinese Academy of Engineering and Higher Education Press Limited Company. This is an open access article under the CC BY license (<http://creativecommons.org/licenses/by/4.0/>).

1. Introduction

Thermal comfort is vital for people's health and safety due to the narrow normal temperature range of the delicate human body system [1,2]. It is generally accepted that the normal temperature range of the human body at rest is only from 36 to 38 °C [3]. Both low and high temperatures have an adverse effect on health and can cause harmful and even life-threatening hypothermia or hyperthermia [4,5]. Furthermore, whether or not a person is experiencing a comfortable thermal condition influences people's psychological state and labor productivity, ultimately affecting social development [6]. Rather than relying on the whole external environment—such as heating, ventilation, and air conditioning (HVAC) systems in buildings [7–9]—to realize people's thermal comfort, the concept of a personal thermal management strategy that focuses on the human body itself and on its local environment is

attracting increasing attention [10–12]. By gaining improved control over heat transport between the human body and its local environment, effective thermoregulation for the human body can be achieved, resulting in enhanced thermal comfort. In turn, a tremendous amount of energy used to maintain the temperature of empty space in buildings and of other objects could be conserved [7,13–15].

As the interface of energy exchange between the human body and the ambient air, clothing plays an important role in the thermal comfort of the human body [16]. With the aim of passively optimizing control over heat dissipation from the human body, novel textile materials have been reported for personal thermal management. Thermal properties have been engineered based on the heat dissipation routes of the human body to facilitate or reduce heat dissipation via specific paths. For example, we recently demonstrated infrared (IR) transparent nanoporous polyethylene (nanoPE) textiles that can maximize the escape of thermal radiation in the mid-IR wavelength range from the human body, resulting in radiative cooling [17–20]. Low-emissivity textiles have also

* Corresponding author.

E-mail address: yicui@stanford.edu (Y. Cui).

been designed that cut down the loss of mid-IR wavelength radiation through clothing, resulting in a warming effect [21,22]. Textiles with engineered heat conduction properties have also been developed to regulate the conductive thermal resistance provided by the clothing system. Materials with high thermal conductivity have been applied as composite fillers, coatings, and so forth in or on textiles to increase the thermal conductance [23–25], while enhanced thermal insulation has been realized, usually by the embedment or addition of microscale or nanoscale air pockets in or on clothing fibers [26–28].

For a clothed human body in a typical indoor environment without perspiration, conduction is the dominating dry heat transport route between the skin and the inner surface of clothing textiles, and within the textile itself, for conventional IR-opaque textiles [21]. Nevertheless, radiation and convection play a more important role in dry heat transfer between the outer surface of textiles and the ambient [13,21]. Therefore, it would be ideal if the entire heat transport pathway from the skin to the ambient could be thoroughly controlled. A combination of superior heat conduction and radiation could expedite heat loss by reducing overall thermal resistance to achieve a cooling effect. Alternatively, diminished heat conduction and radiation could combine to further decrease heat dissipation to achieve a warming effect.

Herein, we propose a bifunctional asymmetric fabric (BAF) for personal cooling and warming based on both tailored heat conduction and tailored radiation properties. Taking advantage of surface roughness asymmetry, a facile modification method was developed for commercially available fabrics to realize a fabric with an overall thermal resistance on one side of the fabric, and a different thermal resistance once the fabric is flipped over. The conceptual design of the BAF is illustrated in Fig. 1. The BAF is an asymmetric fabric with different surface roughness on its two sides. It is modified with heat conductive material that can improve heat conduction between the human body and the inner surface of the fabric, as well as throughout the body of the fabric. A thin layer of high-emissivity (ϵ) material is applied to the rough side of the fabric. When the smooth side is in contact with the skin, heat is conducted through the textile, reaches the high-emissivity outer surface, and is emitted into the ambient efficiently; as a result, a cooling effect is achieved for the person wearing the fabric. Conversely, in the warming mode, when the textile is flipped over and the rough side is in contact with the skin, the air gaps between the rough side and the skin act as an extra thermal insulation layer to decrease heat dissipation via conduction. Meanwhile, the

smooth side with reduced emissivity faces the ambient and increases the radiative thermal resistance, resulting in a personal warming effect.

2. Materials and methods

2.1. Sample preparation

Blank asymmetric fabric with a laminated structure composed of 96% polyester and 4% spandex, with a fabric density of about $220 \text{ g}\cdot\text{m}^{-2}$, was purchased from a commercial website[†]. To prepare the BAF, the blank fabric was first cleaned and then modified with a polydopamine (PDA) coating for 2 h in an aqueous solution consisting of $2 \text{ g}\cdot\text{L}^{-1}$ dopamine hydrochloride (Sigma-Aldrich, USA) and $10 \text{ mmol}\cdot\text{L}^{-1}$ Tris-buffer solution (pH 8.5; Teknova, USA) [29]. For the electroless plating of silver (Ag), the PDA-coated fabric was then dipped into a $25 \text{ g}\cdot\text{L}^{-1}$ AgNO_3 solution (99.9%; Alfa Aesar, USA) for 30 min to form the Ag seed layer. After rinsing with deionized (DI) water, the fabric was immersed in a plating bath solution containing $4.2 \text{ g}\cdot\text{L}^{-1}$ $[\text{Ag}(\text{NH}_3)_2]^+$ (made by adding 28% $\text{NH}_3\cdot\text{H}_2\text{O}$ dropwise into $5 \text{ g}\cdot\text{L}^{-1}$ AgNO_3 until the solution became clear again) and $5 \text{ g}\cdot\text{L}^{-1}$ glucose (anhydrous; EMD Millipore Chemicals, USA) [30] for 2 h. Next, the fabric was turned over and placed into a new plating bath for another 2 h. After Ag plating and drying, oil paint (soft mixing white; Winton, USA) was coated onto the rough side and dried ($\sim 0.29 \text{ g}$ of oil paint was used for 25 cm^2 of fabric) to complete the preparation of the BAF. The Ag fabric and high- ϵ fabric mentioned above were prepared by skipping the steps of adding oil paint or Ag plating, respectively. Cotton fabric for comparison was obtained from a short-sleeve T-shirt (100% cotton, single jersey knit, $\sim 135 \text{ g}\cdot\text{m}^{-2}$, $\sim 400 \mu\text{m}$ thickness; Dockers, USA). A Dri-FIT fabric sample, also for comparison purposes, was obtained from a regular Dri-FIT T-shirt (100% polyethylene terephthalate (PET), single jersey knit, $143 \text{ g}\cdot\text{m}^{-2}$, $\sim 400 \mu\text{m}$ thickness; Nike, USA).

2.2. Material characterization

Scanning electron microscopy (SEM) images were taken using an FEI Nova NanoSEM 450, USA. IR transmittance and reflectance were measured by a Fourier-transform infrared (FTIR) spectrometer (Model 6700; Thermo Scientific, USA) fitted with a diffuse gold integrating sphere (PIKE Technologies, USA). The emissivity was calculated (as $1 - \text{transmittance} - \text{reflectance}$). Thermal images were taken with a thermal camera (EG; FLIR, USA).

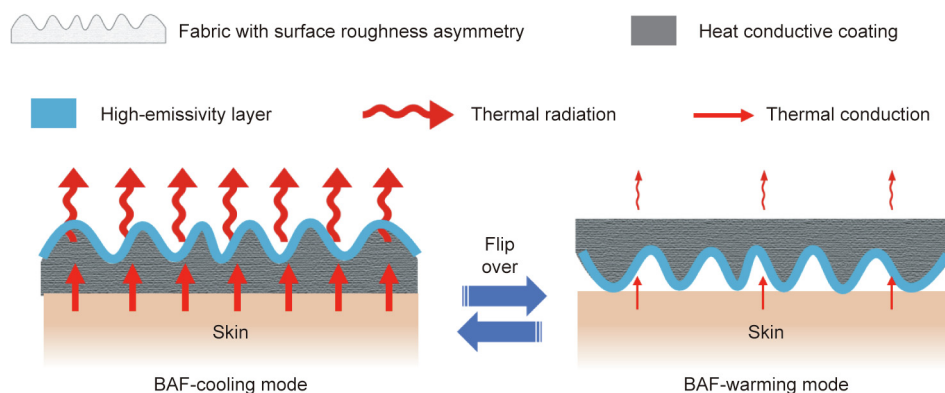


Fig. 1. Conceptual schematic of bifunctional asymmetric fabric (BAF) with tailored thermal conduction and radiation properties for personal cooling and warming. In the cooling mode, heat conduction and radiation are enhanced to facilitate heat transport from the human body to the ambient. In the warming mode, air gaps create extra heat conduction resistance, while reduced surface emissivity reduces heat dissipation from the human body.

[†] <https://www.fabric.com/>.

2.3. Thermal measurement

We used a silicone-rubber flexible electrical heater (72 cm²; Omega Engineering, USA) connected to a power supply (Keithley 2400, USA) as the skin heater. A K-type thermocouple (0.13 mm in diameter; Omega Engineering) was in contact with the top surface of the simulated skin to measure the skin temperature. Another identical heater to the simulated skin was placed underneath the simulated skin to act as a guard heater, with a thermocouple attached on the bottom. The guard heater with the thermocouple was connected to a temperature controller (Omega Engineering). The temperature of the guard heater was always set at the same temperature as the skin heater to ensure that the direction of heat flux of the simulated skin was only upwards. Multiple layers of duct tape, each 220 μm thick, were used to cover the area around the sample and prevent heat loss from the edges. All the devices were enclosed in a chamber made of acrylic boards (McMaster Carr, USA), and the air temperature (ambient temperature) in the chamber was monitored by a K-type thermocouple and controlled at 24.5 °C by a circulating water system. The heating power of the skin heater was set at 150 W·m⁻², which resulted in a simulated bare skin temperature of 33.5 °C. During the measurements, the simulated skin was covered with fabric samples (5 cm × 5 cm). Another K-type thermocouple was placed on the upper surface of the fabrics. All temperature measurements were read after at least 20 min of stabilization.

2.4. Water vapor transmission rate test

The upright cup testing procedure was based on American Society of Testing Materials (ASTM) E96 [31], with modification. Medium bottles (100 mL; Fisher Scientific, USA) were filled with 80 mL distilled water and sealed with fabric samples using open-top caps and silicone gaskets (Corning, USA). The exposed area of the fabrics was 3 cm in diameter. The sealed bottles were placed into an environmental chamber (BTU-133; Espec, USA) in which the temperature was held at 35 °C and the relative humidity at 30% ± 5%. The mass of the bottles and the samples was measured periodically. By dividing the reduced mass of the water by the exposed area of the bottle, the water vapor transmission was calculated.

2.5. Air permeability test

The testing procedure was based on ASTM D737 [32], with modification. The fabric sample was fixed between two pipes using a flange adapter, a centering O-ring and a clamp. The exposed area was 1.65 cm in diameter. One pipe was connected to a T-connector at the short/straight leg and then connected to the compressed air source. A flowmeter (Dwyer, USA; maximum flow rate: 25 L·min⁻¹) was placed between the compressed air source and the T-connector. The other pipe was also connected to a T-connector at the short/straight leg and then connected to the open air. A differential pressure gauge (UEi Test Instruments, USA) was connected to both the long/branch legs to measure the pressure drops across the fabric sample at different air flow rates. The linear velocity of the air flow was calculated using the air flow rate divided by the exposed area.

2.6. Washing test

The BAF (5 cm × 5 cm) was placed in a 100 mL bottle filled with 80 mL distilled water and 0.2 g laundry detergent (Tide, USA). A stir bar was utilized to stir the solution at the speed of 500 r·min⁻¹. The BAF was washed for 30 min (one cycle) and 50 h (100 cycles). The solution before washing and after washing for one cycle and 100

cycles was collected, diluted by 5 vol% nitric acid, and tested by inductively coupled plasma spectrometry (ICP-MS) to quantify the Ag mass loss during washing. After washing for 50 h, the BAF was dried, and the surface emissivity measurement and simulated skin thermal measurement were performed again.

3. Results and discussion

3.1. The BAF fabrication

To demonstrate the concept, the BAF was fabricated via the process shown in Fig. 2(a). We adopted a commercial fabric with a laminated structure, which resulted in asymmetric surface structures (Fig. S1 in Appendix A). The BAF has a relatively rough surface on one side and a smooth surface on the other, which matches the desired structure in our conceptual design. The asymmetric structure is clearly visible in the SEM image of the fabric (Appendix A Fig. S2). It should be noted that the selection of this fabric is not fixed; the fabric can be replaced by other fabrics with similar structures, or an asymmetric fabric can be made by laminating one conventional fabric layer to another, thereby creating artificial humps. We took the blank asymmetric fabric as the substrate. Electroless plating was utilized to coat Ag onto the fibers in the fabric as the heat conductive coating. Fig. S3 in Appendix A exhibits photographs of the Ag-coated fabric (denoted as “Ag fabric”). Finally, we used oil paint to add a thin high-emissivity layer on the rough side. The as-fabricated BAF is shown in Figs. 2(b) (smooth side) and (c) (rough side). The surface morphology of the BAF was characterized by SEM, which revealed that the Ag coating is conformal and completely covers the fibers' surface, as shown in Figs. 2(d) and (e). The cross-section SEM image of the Ag fabric verifies that the Ag coating was applied onto every fiber inside the fabric without blocking the pores among the fibers (Appendix A Fig. S4). On the smooth side of the fabric, the surface of the fibers on the top is covered with oil paint, but the gaps among the fibers are well preserved (Figs. 2(f) and (g)). Moreover, the high-emissivity modification layer only penetrates tens of micrometers into the fabric surface, as displayed in the magnified cross-section SEM image of the BAF near the rough side (Appendix A Fig. S5).

3.2. IR light emissivity and thermal measurements

The total IR light emissivity was investigated with an FTIR spectrometer equipped with a diffuse gold integrating sphere. The transmittance (τ) and reflectance (ρ) of the BAF surfaces in the mid-IR wavelength range were measured, and the emissivity was calculated by means of $1 - \tau - \rho$. As displayed in Fig. 3(a), without surface modification, the blank asymmetric textile had almost identical emissivity from its rough side and smooth side. The Ag coating decreased the surface emissivity on both sides. Even though Ag is an excellent low-emissivity material (ϵ : 0.02–0.03) [33], the rough substrates such as fabrics made by the weaving or knitting of fiber or yarn can dramatically increase the final emissivity [34]. This is why the measured emissivity of the Ag fabric was greater than that of bulk Ag. Nevertheless, the emissivity difference on the two sides of the fabric with different roughness was evident. The relatively rougher side exhibited higher emissivity, while the emissivity of the smooth side of the BAF was the same as that of the smooth side of the Ag-coated fabric. In contrast, the rough side of the BAF exhibited very high emissivity (approximately 0.95) over a wide range of wavelengths due to the addition of a high-emissivity layer.

To characterize the heat conduction property of the fabric, we measured the temperature difference (ΔT) between the simulated skin surface (T_{skin}) and the outer surface of the fabric (T_{top}), using

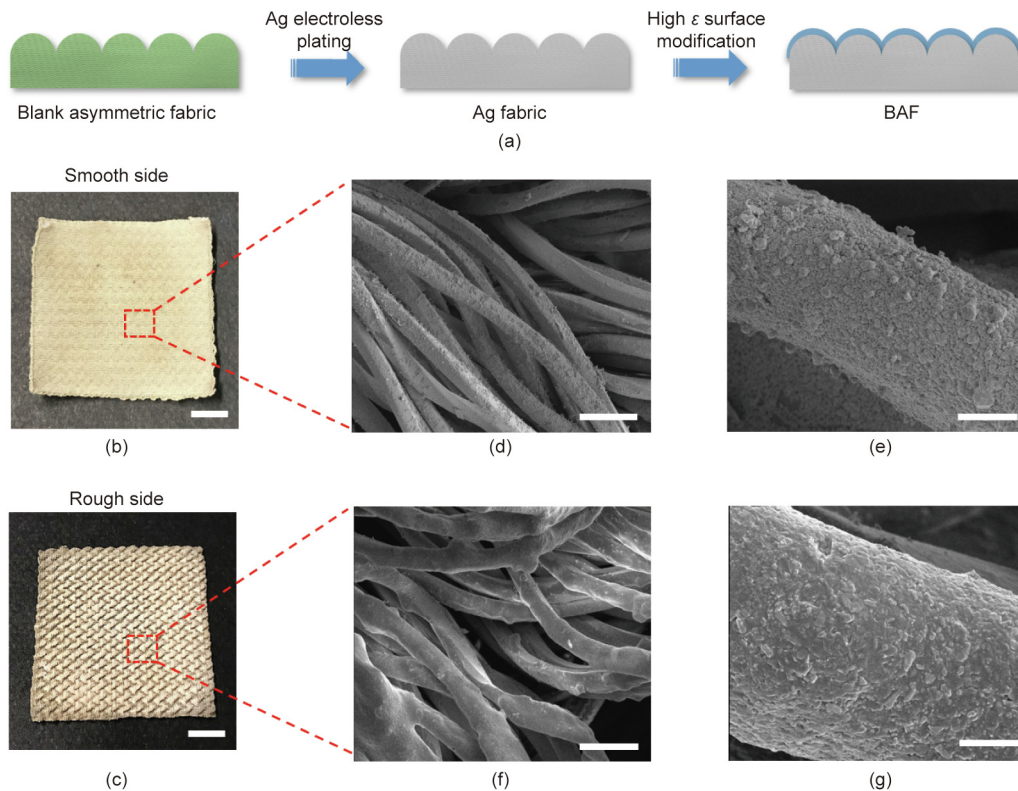


Fig. 2. BAF fabrication and surface morphology. (a) Schematic of the BAF fabrication process. Laminated fabric with asymmetric surface roughness underwent Ag electroless plating to obtain heat conductive Ag coating on its fibers. A thin high-emissivity layer was then added onto the rough side. (b, c) Photographs of (b) the smooth side and (c) the rough side of the as-fabricated BAF (scale bars: 1 cm). (d) SEM image of the smooth side of the BAF (scale bar: 50 μm). (e) Magnified SEM image of the smooth side of the BAF (scale bar: 5 μm). (f) SEM image of the rough side of the BAF (scale bar: 50 μm). (g) Magnified SEM image of the rough side of the BAF (scale bar: 5 μm).

the simulated skin thermal measurement, as illustrated in Fig. 3(b). The power density of the skin heater was maintained at a constant level, and the temperature of the guard heater was continually adjusted to be identical to the skin temperature in order to prevent downward heat flux. The entire measurement system was enclosed by a chamber at a stable temperature, controlled by a circulating water system. As shown in Fig. S6 in Appendix A, ΔT can be taken as an index showing the overall heat transportation capacity from the skin to the upper surface of the fabric, in which heat conduction is the dominant heat transport route. The measurement results are displayed in Fig. 3(c). “High- ϵ fabric” refers to the fabric with a high-emissivity modification layer only on the rough side but without an Ag coating. An additional 1.1–1.7 $^{\circ}\text{C}$ ΔT was observed when the smooth side faced up, compared with the measurement when the rough side faced up. This finding reveals that the addition of an air gap effectively creates extra conduction thermal resistance when the rough side comes into contact with skin. It also demonstrates that the Ag coating can decrease the total thermal resistance from the skin to the outer surface of the textile, since the samples with Ag coating (i.e., the Ag fabric and BAF) exhibited a smaller ΔT . It is worth noting that heat transport change via conduction might not be the only factor causing a varied ΔT . Even though heat conduction dominated the overall heat transport, change in other heat transfer routes, such as radiation, may still contribute.

Furthermore, we measured the simulated skin temperature with fabric samples in different modes to characterize the comprehensive thermal effect, as shown in Fig. 3(d). The blank fabric with the smooth side coming into contact with the skin (i.e., rough side up) was regarded as a benchmark, since all the modifications were based on the blank fabric, and since conventional fabrics usually contact the skin with a similar smooth surface. In the cooling mode (rough side up), the BAF exhibited around 2.6 $^{\circ}\text{C}$ lower skin tem-

perature than the blank fabric, due to the combination of enhanced heat conduction and enhanced radiation. Due to the decrease in surface emissivity, the Ag fabric did not present a significant cooling effect, even though it was more heat conductive than the blank fabric. Furthermore, the fabric that only had high-emissivity modification was unable to achieve a cooling effect comparable to that of the BAF. These facts verify that the combination of tailored heat conduction and radiation with a focus on the whole heat transport pathway from the skin to the ambient is more effective for personal cooling than the application of only one or the other of these methods. In the warming mode, flipping over the blank fabric resulted in a skin temperature of about 1.2 $^{\circ}\text{C}$ higher because of the extra air gap introduced by the asymmetric structure roughness. A reinforced warming effect was also realized through the addition of the lower emissivity outer surface. Accordingly, the BAF in the warming mode resulted in an approximately 2 $^{\circ}\text{C}$ warming effect compared with the benchmark. As a result, the surface modifications expand the skin temperature difference between the cooling mode and the warming mode to 4.6 $^{\circ}\text{C}$, indicating that the thermal comfort zone can increase by 4.6 $^{\circ}\text{C}$ with a single piece of BAF, compared with conventional fabrics with a symmetrical structure.

We utilized an IR camera to visualize the thermal effect of fabric samples placed on the same simulated skin at 35 $^{\circ}\text{C}$ (Fig. 3(e)). The actual upper surface temperature and its emissivity, taken together, determined the apparent temperature in the thermal image [35]. For the blank fabric, the air gap caused a temperature decrease in the upper surface when the smooth side faced up, so its thermal image looks colder than the image with the rough side facing up. In cooling mode, the BAF decreased the temperature difference between the simulated skin and its upper surface. With higher emissivity, the BAF temperature in the thermal image appears to be the highest. In contrast, in the warming mode, the lower surface temperature of the BAF, caused by greater

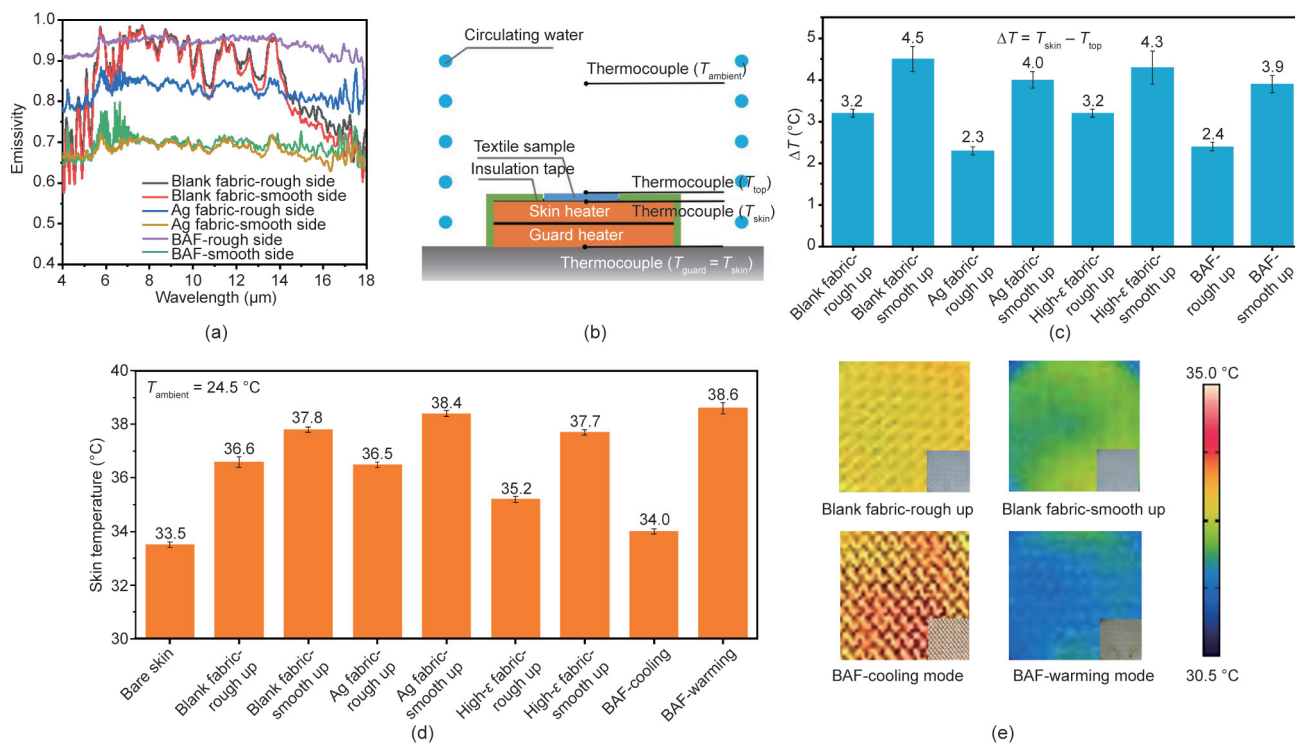


Fig. 3. Surface emissivity characterization and thermal measurements of the BAF. (a) Surface emissivity of both sides of the blank fabric, Ag fabric, and BAF in the mid-IR wavelength range. “Ag fabric” refers to the asymmetric fabric with only an Ag coating modification. (b) Schematic of the thermal measurement apparatus, in which the ambient temperature and skin heater power density were set to be constant and the guard heater temperature was always the same as the skin heater. (c) Temperature difference between skin and the upper surface of the fabric for the fabrics in varied modes, showing the overall heat transport resistance from the skin to the upper surface of the fabric. “High-ε fabric” refers to the asymmetric fabric with only a high-emissivity modification on the rough side. (d) Simulated skin temperature with different fabrics in varied modes in the thermal measurement. (e) IR thermal images for the blank asymmetric fabrics and BAF placed on a simulated skin at 35 °C. The squares at the bottom right of the four panels show the optical photographs of the fabric surfaces.

conduction thermal resistance and its low emissivity, render it much colder in the thermal image.

3.3. Wearability tests

After the demonstration of the thermoregulation ability of the BAF for both personal cooling and warming, the wearability of the BAF was evaluated. The BAF was fabricated via surface modification from commercialized fabric, whose wearability can be considered to be fair enough for daily wearing. Hence, we focused on checking the features that were the most likely to be damaged by the surface modifications. Fig. 4(a) exhibits the water vapor transmission test results of the BAF, blank asymmetric fabric, fabric from a cotton T-shirt, and fabric from a Dri-FIT T-shirt. The water vapor transmission rate of the BAF is comparable to that of the blank asymmetric fabric, indicating that the surface modifications merely impacted the original water vapor transmission ability. Both fabrics also show a similar water vapor transmission rate to that of the cotton and Dri-FIT, both of which are widely accepted as fabrics with a reasonable water vapor transmission rate. This finding also verifies that the laminated fabric structure with asymmetric surface roughness can exhibit as high a water vapor transmission rate as that of conventional fabrics. The air permeability of these four fabrics was also investigated; all four show comparable good air permeability (Fig. 4(b)). Furthermore, we performed a washing test for the BAF, where 30 min of washing in water with detergent was defined as a cycle. The washing solution after one cycle and after 100 cycles was analyzed by means of ICP-MS to quantify the Ag loss. One cycle of washing was found to cause about 0.20% Ag loss, while washing for 100 cycles resulted in about 0.38% Ag loss (Fig. 4(c)). This finding indicated that the Ag loss amount from washing is very minimal, and the BAF can sustain

the Ag coating well after washing during practical use. The surface emissivity of both sides of the fabric was probed again after 100 cycles of washing. As exhibited in Fig. 4(d), the emissivity of either side of the fabric was comparable to that before washing. We also reperformed the simulated skin thermal measurement to identify its cooling/warming effect. After 100 cycles of washing, the measured skin temperature in the test remained nearly the same (Fig. 4(e)).

4. Conclusions

In summary, we demonstrated the development of a BAF with tailored heat conduction and radiation properties for personal cooling and warming via a facile surface modification method. Enhanced thermoregulation capacity was realized by means of simultaneous engineered heat conduction and radiation, which provide improved control over the entire heat transport pathway from the skin to the ambient. With the advantages provided by the surface roughness asymmetry and the proposed surface modification method, the BAF realizes both effective personal cooling and effective personal warming, and can expand the thermal comfort zone by 4.6 °C for the human body with a single piece of clothing. We expect that this work will provide new insights for the design of personal thermal management textiles as well as a novel solution for the facile modification of available fabrics for both personal cooling and warming.

Acknowledgments

Part of this work was performed at the Stanford Nano Shared Facilities and the Stanford Nanofabrication Facility. The authors thank S. Fan for lending the thermal camera.

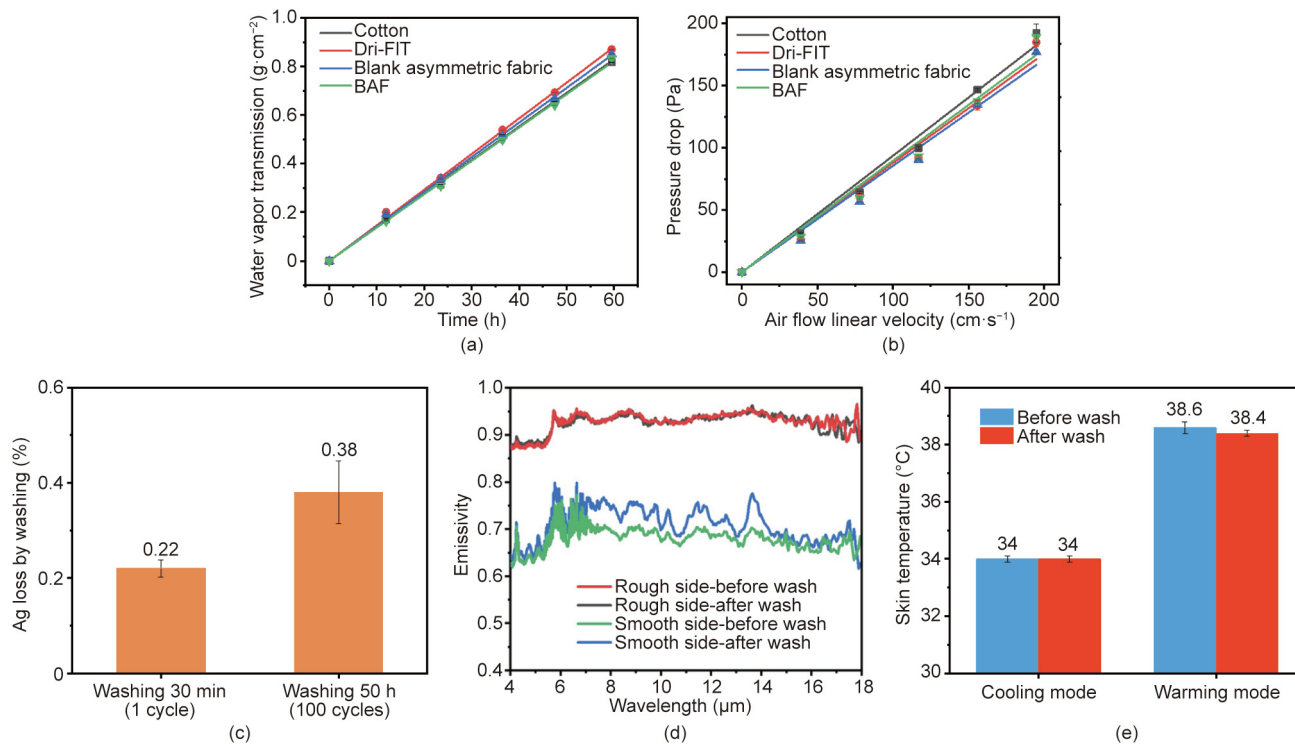


Fig. 4. Wearability tests of the BAF. (a) Water vapor transmission rate test showing the transmission speed of water vapor generated from the human body through the fabric. (b) Air permeability test measuring how well the fabric allows the passage of air. (c) Ag loss ratio of the BAF after washing, as measured by ICP-MS. (d) Measured surface emissivity of both sides before and after 100 cycles of washing. (e) Measured skin temperature during the simulated skin thermal measurement for both the cooling and warming modes before and after 100 cycles of washing.

Compliance with ethics guidelines

Yucan Peng, Hiang Kwee Lee, David S. Wu, and Yi Cui declare that they have no conflict of interest or financial conflicts to disclose.

Appendix A. Supplementary data

Supplementary data to this article can be found online at <https://doi.org/10.1016/j.eng.2021.04.016>.

References

[1] Xiong J, Lian Z, Zhou X, You J, Lin Y. Effects of temperature steps on human health and thermal comfort. *Buill Environ* 2015;94:144–54.
 [2] Djongyang N, Tchinda R, Njomo D. Thermal comfort: a review paper. *Renew Sustain Energy Rev* 2010;14(9):2626–40.
 [3] Goldstein LS, Dewhirst MW, Repacholi M, Kheifets L. Summary, conclusions and recommendations: adverse temperature levels in the human body. *Int J Hyperthermia* 2003;19(3):373–84.
 [4] Desforges JF, Simon HB. Hyperthermia. *N Engl J Med* 1993;329(7):483–7.
 [5] Sosnowski P, Mikrut K, Krauss H. Hypothermia—mechanism of action and pathophysiological changes in the human body. *Postepy Hig Med Dosw* 2015;69:69–79. Polish.
 [6] Chan APC, Yi W. Heat stress and its impacts on occupational health and performance. *Indoor Built Environ* 2016;25(1):3–5.
 [7] Hoyt T, Arens E, Zhang H. Extending air temperature setpoints: simulated energy savings and design considerations for new and retrofit buildings. *Buill Environ* 2015;88:89–96.
 [8] Sadineni SB, Madala S, Boehm RF. Passive building energy savings: a review of building envelope components. *Renew Sustain Energy Rev* 2011;15(8):3617–31.
 [9] Yang L, Yan H, Lam JC. Thermal comfort and building energy consumption implications—a review. *Appl Energy* 2014;115:164–73.
 [10] Zhang XA, Yu S, Xu B, Li M, Peng Z, Wang Y, et al. Dynamic gating of infrared radiation in a textile. *Science* 2019;363(6427):619–23.
 [11] Tong JK, Huang X, Boriskina SV, Loomis J, Xu Y, Chen G. Infrared-transparent visible-opaque fabrics for wearable personal thermal management. *ACS Photonics* 2015;2(6):769–78.

[12] Hsu PC, Liu X, Liu C, Xie X, Lee HR, Welch AJ, et al. Personal thermal management by metallic nanowire-coated textile. *Nano Lett* 2015;15(1):365–71.
 [13] Peng Y, Cui Y. Advanced textiles for personal thermal management and energy. *Joule* 2020;4(4):724–42.
 [14] Yang B, Ding X, Wang F, Li A. A review of intensified conditioning of personal micro-environments: moving closer to the human body. *Energy Built Environ* 2021;2(3):260–70.
 [15] Ghahramani A, Zhang K, Dutta K, Yang Z, Becerik-Gerber B. Energy savings from temperature setpoints and deadband: quantifying the influence of building and system properties on savings. *Appl Energy* 2016;165:930–42.
 [16] Yu W. Achieving comfort in intimate apparel. In: Song G, editor. *Improving comfort in clothing*. Cambridge: Woodhead Publishing Limited; 2011. p. 427–48.
 [17] Hsu PC, Song AY, Catrysse PB, Liu C, Peng Y, Xie J, et al. Radiative human body cooling by nanoporous polyethylene textile. *Science* 2016;353(6303):1019–23.
 [18] Peng Y, Chen J, Song AY, Catrysse PB, Hsu PC, Cai L, et al. Nanoporous polyethylene microfibres for large-scale radiative cooling fabric. *Nat Sustain* 2018;1(2):105–12.
 [19] Cai L, Peng Y, Xu J, Zhou C, Wu P, et al. Temperature regulation in colored infrared-transparent polyethylene textiles. *Joule* 2019;3(6):1478–86.
 [20] Cai L, Song AY, Li W, Hsu PC, Lin D, Catrysse PB, et al. Spectrally selective nanocomposite textile for outdoor personal cooling. *Adv Mater* 2018;30(35):1802152.
 [21] Cai L, Song AY, Wu P, Hsu PC, Peng Y, Chen J, et al. Warming up human body by nanoporous metallized polyethylene textile. *Nat Commun* 2017;8(1):496.
 [22] Hsu PC, Liu C, Song AY, Zhang Ze, Peng Y, Xie J, et al. A dual-mode textile for human body radiative heating and cooling. *Sci Adv* 2017;3(11):e1700895.
 [23] Abbas A, Zhao Y, Wang X, Lin T. Cooling effect of MWCNT-containing composite coatings on cotton fabrics. *J Textil Inst* 2013;104(8):798–807.
 [24] Manasoglu G, Celen R, Kanik M, Ulcay Y. Electrical resistivity and thermal conductivity properties of graphene-coated woven fabrics. *J Appl Polym Sci* 2019;136(40):48024.
 [25] Gao T, Yang Z, Chen C, Li Y, Fu K, Dai J, et al. Three-dimensional printed thermal regulation textiles. *ACS Nano* 2017;11(11):11513–20.
 [26] Cui Y, Gong H, Wang Y, Li D, Bai H. A Thermally insulating textile inspired by polar bear hair. *Adv Mater* 2018;30(14):1706807.
 [27] Wang Z, Zhong Y, Wang S. A new shape factor measure for characterizing the cross-section of profiled fiber. *Text Res J* 2012;82(5):454–62.

- [28] Jabbari M, Åkesson D, Skrifvars M, Taherzadeh MJ. Novel lightweight and highly thermally insulative silica aerogel-doped poly(vinyl chloride)-coated fabric composite. *J Reinf Plast Compos* 2015;34(19):1581–92.
- [29] Lee H, Dellatore SM, Miller WM, Messersmith PB. Mussel-inspired surface chemistry for multifunctional coatings. *Science* 2007;318(5849):426–30.
- [30] Hsu PC, Kong D, Wang S, Wang H, Welch AJ, Wu H, et al. Electrolessly deposited electrospun metal nanowire transparent electrodes. *J Am Chem Soc* 2014;136(30):10593–6.
- [31] ASTM International. E96/E96M-16: Standard test methods for water vapor transmission of materials. ASTM standards. West Conshohocken: American Society of Testing Materials International; 2016.
- [32] ASTM International. D737-18: Standard test method for air permeability of textile fabrics. West Conshohocken: American Society of Testing Materials International; 2018.
- [33] Woods SI, Jung TM, Sears DR, Yu J. Emissivity of silver and stainless steel from 80K to 300K: application to ITER thermal shields. *Cryogenics* 2014;60:44–8.
- [34] Wen CD, Mudawar I. Modeling the effects of surface roughness on the emissivity of aluminum alloys. *Int J Heat Mass Transf* 2006;49(23-24):4279–89.
- [35] Fragopoulou A, Institutet K, National M. Infrared thermography imaging: evaluating surface emissivity and skin thermal response to IR heating infrared thermography imaging. *e-J Sci Technol* 2016;3:9–14.